ACS APPLIED MATERIALS & INTERFACES

Research Article

www.acsami.org

Core–Shell Ti@Si Coaxial Nanorod Arrays Formed Directly on Current Collectors for Lithium-Ion Batteries

Xinghua Meng and Da Deng*

Department of Chemical Engineering and Materials Science, Wayne State University, 5050 Anthony Wayne Drive, Detroit, Michigan 48202, United States

Supporting Information

ABSTRACT: Silicon is a promising candidate to replace the dominantly used carbon as the anode material for lithium ion batteries (LIBs). Si has the highest theoretical capacity (4200 mA·h/g) and is one of the most abundant elements. Unfortunately, Si has the issues of huge volume variation upon dis/charge cycling and low conductivity, leading to poor cycling and rate performances. Designing special nanostructures and improving conductivity and integration of Si electrodes could dramatically enhance their performance. Here, we introduce a novel strategy to integrate the core–shell nanorod arrays of Ti@Si on Ti foil with good conductivity as an additive-free electrode. The Ti core functions as a stable metallic support for the Si shell and dramatically reduces the diffusion length. The as-prepared core–shell nanorod arrays of Ti@Si on Ti foil, without any postsynthesis treatment, as electrodes demonstrated reversible capacity of 1125 mA·h/g over at least 30 cycles with highly improved Coulombic efficiency.

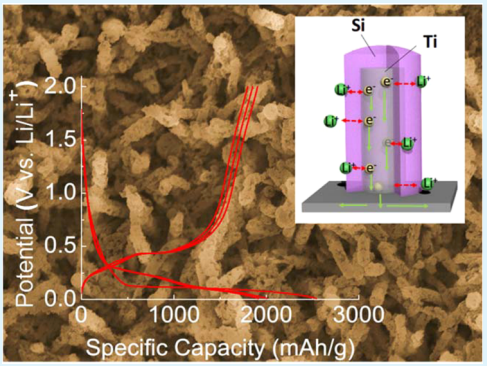

KEYWORDS: *Ti@Si core–shell, coaxial nanorod, silica, magnesiothermic, lithium-ion batteries*

INTRODUCTION

Lithium-ion batteries (LIBs) are dominantly used in mobile electronics and are playing an increasing role in electric vehicles. Another emerging market for LIBs will be energy storage for renewable but intermittent energy, such as sustainable solar and wind energy.[1] To meet the increasing demand for high-energy LIBs, next-generation LIBs with dramatically improved electrochemical performance must be developed. The electrochemical performance of LIBs is determined by the electrode materials selected. Taking the anode for example, carbon-based anodes are exclusively used in LIBs and the theoretical capacity is about 372 mA·h/g (based on LiC_6). However, the performance of carbon anodes is almost saturated after two decades of research and development since Sony first commercialized LIBs. Therefore, it is crucial to develop carbon-alternative anodes with high capacity for next-generation LIBs.

Silicon is one of the most desirable carbon-alternative anode candidates. Silicon has the highest theoretical specific capacity (4200 mA·h/g based on $Li_{4.4}Si$) among all anode materials for LIBs.[1] Unfortunately, Si has poor cyclability due to the pulverization caused by huge volume change (400%) upon the insertion–extraction of lithium ions.[2,3] Another issue with Si, a semiconductor, is that its conductivity is poor.[4] The low conductivity negatively impacts electron transport, leading to poor utilization of the active materials, much lower capacity than its theoretical value, and low battery charging rates.

We tried to address the issues associated with silicon anodes for LIBs by designing a unique structure with Ti@Si core–shell coaxial nanorod arrays on a current collector for LIBs. A facile procedure was developed to synthesize the coaxial nanorod arrays. The porous silicon shells supported by metallic Ti cores could accommodate volumetric variation. Meanwhile, the metallic Ti cores could enhance the conductivity of the Si shells. The schematic of the procedure involved and changes in compositions are illustrated in Figure 1.

We used TiO_2 nanorod arrays grown on titanium foils prepared by a hydrothermal method as the template and precursor. Next, the TiO_2@SiO_2 core–shell coaxial nanorod arrays were obtained by coating the TiO_2 nanorod arrays with silica by a sol–gel method. Subsequently, both the silica shells and TiO_2 cores were reduced to Si shells and metallic Ti cores, respectively, by magnesiothermic reduction. The MgO by-product could be removed by HCl etching easily. The as-prepared Ti@Si core–shell nanorod arrays formed on metallic titanium foils could be used for battery assembly without any additional treatment. It should be highlighted that the reduction of TiO_2 to metallic Ti cores is highly beneficial from the perspective of enhanced conductivity.[5,6] The as-prepared, not-optimized Ti@Si core–shell nanorod arrays demonstrated impressive electrochemical performance in reversible lithium storage. Our preliminary results show that a highly reversible capacity of 1125 mA·h/g over 30 cycles at testing current of 200 mA/g could be achieved.

Received: January 17, 2015
Accepted: March 6, 2015
Published: March 6, 2015

DOI: 10.1021/acsami.5b00492
ACS Appl. Mater. Interfaces 2015, 7, 6867–6874

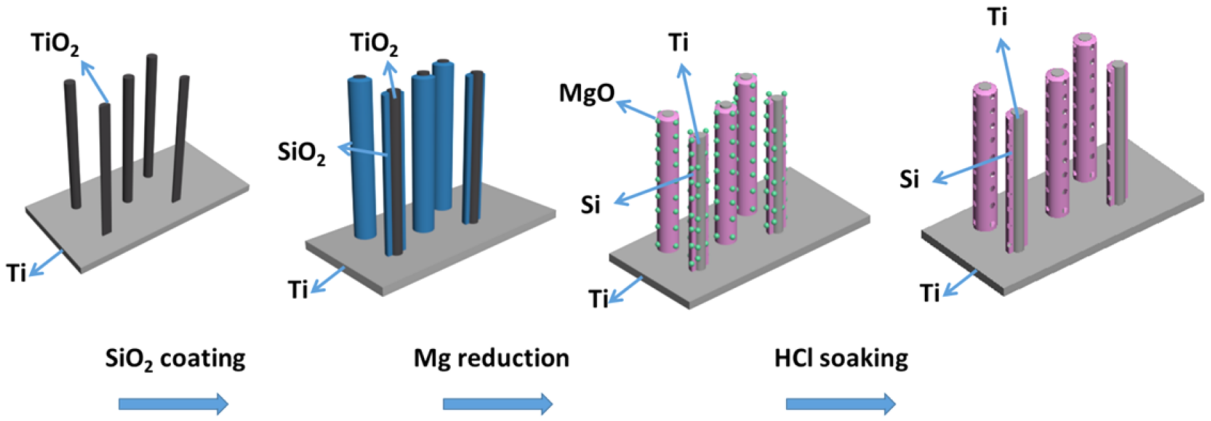

Figure 1. Schematic to illustrate the changes in structures and compositions at different stages of synthesis.

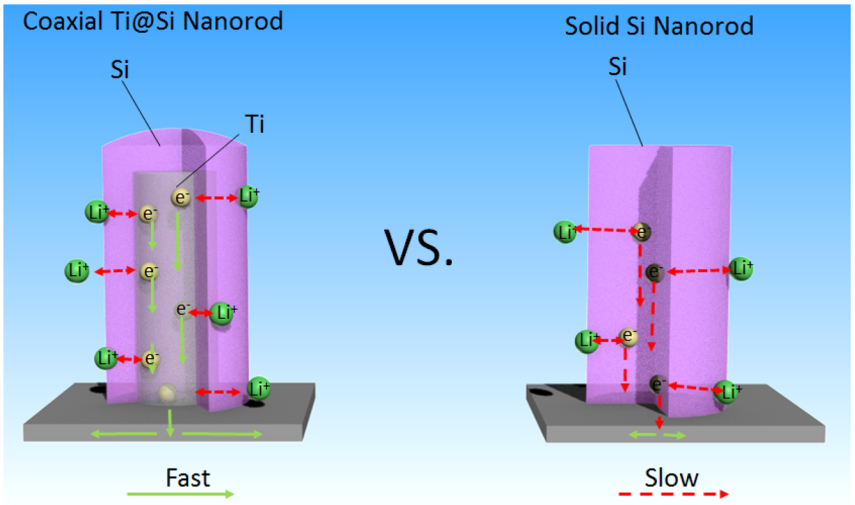

Figure 2. Schematic to illustrate the advantages of Ti@Si core–shell coaxial nanorod (left) as compared with solid Si nanorod (right) in facilitating both ion and electron transfer.

EXPERIMENTAL SECTION

Preparation of TiO_2 Nanorod Arrays on Metallic Ti Substrate as Precursor. The preparation follows a modified procedure.[7] Typically, a piece of Ti foil (0.5 × 0.5 cm^2) was put into an aqueous NaOH solution (0.25 M) inside a Teflon-lined autoclave. The reactor was heated to 220 °C, maintained at the set temperature for 24 h, and then cooled down to room temperature naturally. The treated foil was then immersed in a dilute HCl solution (0.6 M) for 1 h to exchange the Na ions with protons, rinsed with a copious amount of water, and dried under ambient conditions. The samples were then heated at 600 °C for 2 h inside a furnace in air.

Fabrication of SiO_2@TiO_2 Core–Shell Coaxial Nanorod Arrays on Ti Substrate. Typically, the previously prepared TiO_2 nanorod arrays on Ti foils were put into 2-propanol (30 mL) inside a round-bottom flask. Under stirring, 4 mL of deionized water was added, followed by 3 g of tetraethyl orthosilicate (TEOS) and further stirred. Then, 1 mL of saturated ammonia solution was added consecutively in portions with a pipet. The mixed solution was further stirred for 6 h. The SiO_2-coated TiO_2 nanorod arrays were washed by water and ethanol repeatedly and then dried at 300 °C for 2 h in air.

Fabrication of Ti@Si Core–Shell Coaxial Nanorod Arrays on Ti Substrate. The previously prepared TiO_2@SiO_2 core–shell coaxial nanorod arrays on Ti foils were put inside a crucible and 50 mg of Mg powder was spread beneath and on top of two pieces of the treated foils, and an additional 50 mg of Mg powder was put near the foils' upper stream in the same crucible. The excess amount of Mg powder was used to achieve complete reduction of SiO_2. The crucible was then inserted into a tube furnace and temperature was ramped from room temperature to 650 °C in 1 h and maintained at the set temperature for 4 h under the protection of argon flowing at a rate of 100 sccm. The foils were soaked in a copious amount of 0.5 M HCl solution to remove extra Mg and MgO and then dried in a vacuum oven. Note that no HF was used here as we assumed that no significant amount of SiO_2 remained, and HF could etch off metallic Ti according to $Ti + 6HF = [TiF_6]^{2-} + 2H^+ + 2H_2\uparrow$.

Material Characterization and Electrochemical Analysis. X-ray diffraction (XRD) analysis of the samples was carried out on a XRD instrument (Rigaku with Cu Kα radiation. λ = 1.540 56 Å). The morphology and microstructures of the as-prepared samples were characterized by field emission scanning electron microscopy (FESEM; JEOL 7600 coupled with energy-dispersive X-ray spectroscopy, EDX), with accelerating voltage of 15 kV and transmission electron microscopy (TEM; JEOL 2010 coupled with EDX under accelerating voltage of 200 kV). Raman spectra were collected on a Jobin-Yvon Horiba Triax 550 Raman spectrometer. An argon-ion laser (514.5 nm) was used as an excitation source. The as-prepared Ti@Si core–shell coaxial nanorod arrays as ready electrodes were assembled into 2032 coin cells. The assembly was carried out inside an argon-filled glovebox with the Ti@Si core–shell coaxial nanorod arrays on Ti foil as the working electrode, metallic lithium foil as the counter and reference electrode, 1 M solution of $LiPF_6$ in a 50:50 (v/v) mixture of ethylene carbonate (EC) and diethyl carbonate (DEC) as the electrolyte, and polypropylene/polyethylene/polypropylene (PP/PE/PP) trilayer membranes (Celgard 2320) as the separator. Electrochemical performance was evaluated by cyclic voltammetry (CV) on an electrochemical workstation (CHI 660D) at a scan rate of 0.1 mV/

DOI: 10.1021/acsami.5b00492
ACS Appl. Mater. Interfaces 2015, 7, 6867–6874

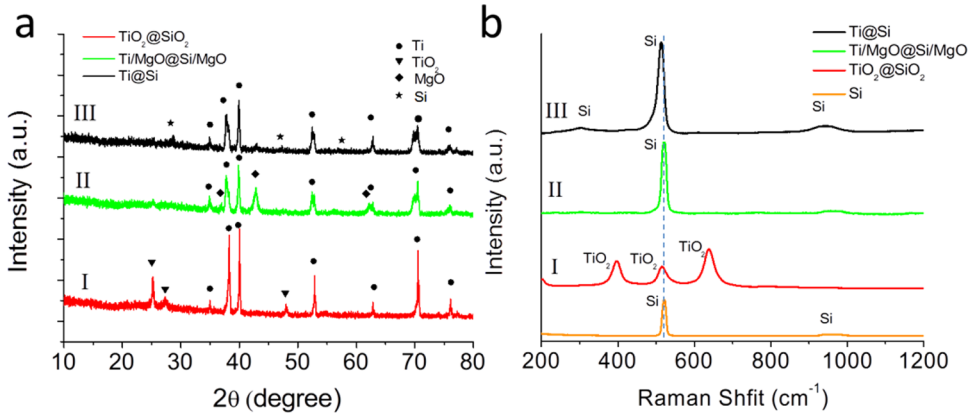

Figure 3. (a) XRD patterns and (b) Raman spectra of different nanorod samples obtained at each stage of preparation. Sample I is the TiO_2@SiO_2 nanorod arrays after silica coating of TiO_2 nanorod arrays; sample II is the Ti/MgO@Si/MgO nanorod arrays after magnesiothermic readuction treatment of I; sample III is the Ti@Si nanorod arrays after HCl treatment to remove MgO of sample II. The orange color Raman spectrum is from a typical Si wafer.

s. The coin cells were charged and discharged galvanostatically at room temperature in the voltage window 0.01−2 V at a current of 200 mA/g on a MTI BST8-WA battery tester.

RESULTS AND DISCUSSION

The advantages of this structure of Ti@Si core−shell coaxial nanorods as compared to bare Si nanorods are illustrated in Figure 2. The obvious benefit of metallic core is that the axial resistance observed in solid Si nanorod could be dramatically reduced. The charges released/acquired on electrochemical reactions of dealloying/alloying for Li_xSi could be transferred to the Ti foil current collectors easily via the metallic Ti nanorod core, in contrast to the solid semiconductor Si nanorod. The incorporation of metallic Ti core could dramatically reduce the Li diffusion distances from the radius of the solid Si nanorod to just the thickness of the shell of the core−shell Ti@Si nanorod. Additionally, the longitudinal direction charge transfer of the semiconductor solid Si nanorod with length of a few micrometers is avoided in the case of coaxial nanorod with metallic core. The distance of charge transfer is reduced to thickness of the shell in the case of Ti@Si core−shell coaxial nanorods. Besides, the contact surface of Si with Ti increases, which could improve the connection between active materials and the collector, if one treats the Li-inactive metallic Ti nanorods as part of the current collector or 3-D nanostructured current collector.

The feasibility of our designed procedure was demonstrated by thorough characterization of the intermediate and final products outlined in Figure 1. The changes in chemical composition for products obtained from different stage of treatment were characterized by X-ray diffraction (XRD) (Figure 3a). The chemical composition of the hydrothermally obtained anatase TiO_2 nanorod arrays has been well-documented and was not further characterized here.[8] Upon coating with silica, only anatase-phase TiO_2 (JCPDS 21-1272) of the nanorod arrays and metallic Ti (JCPDS 44-1294) of the Ti foil were detected, the same as those without SiO_2 coating. This observation suggested that the process of silica coating has not changed the chemical composition of the precursor TiO_2 nanorod arrays on Ti foil. The silica shell is amorphous. After Mg reduction, peaks associated with MgO (JCPDS 45-0946) appeared. The O in MgO must come from the SiO_2 and TiO_2, as the reactions occurred under the protection of inert argon. Given the excess of Mg in the reactor and low melting point of Mg, the Mg vapor could penetrate inside the space between nanorod arrays to completely reduce all the nanoarrays, from the base to the tips. Magnesiothermic reduction to prepare silicon from silica is highly effective and can preserve the nanoscale morphology of the silica precursor.[9−15] At the same time, TiO_2 was converted to metallic Ti via the magnesiothermic reduction. The magnesiothermic reduction of TiO_2 nanorod into metallic Ti nanorods has not been reported before, although the process has been explored for the metallurgical production of bulk metallic Ti with low oxygen content.[16] The melting points for Mg, Si, and Ti are 650, 1414, and 1668 °C, respectively. Therefore, under our experimental conditions of 650 °C, the freshly converted Si and Ti would still be in solid state, and the 1-D feature of nanoarrays before reduction could be preserved. The possible chemical reactions involved are as follows:

$$\text{For } SiO_2 \text{ shell:} \quad 2Mg + SiO_2 \rightarrow 2MgO + Si$$

$$\text{For } TiO_2 \text{ core:} \quad 2Mg + TiO_2 \rightarrow 2MgO + Ti$$

The MgO could be easily etched off by use of a dilute HCl solution. The XRD pattern shows dramatically reduced peaks associated with MgO after washing with HCl solution. The Si peaks are observed, and the weak peaks of Si could be assigned to diffraction from (111), (220), and (311) planes. The broad and weak XRD peaks associated with Si suggest that the coated silicon might be polycrystalline and amorphous silicon. The weak XRD peaks of Si phase at the presence of other dominant phase (e.g., mesocarbon microbeads, MCMB) have been observed before.[17]

The successful magnesiothermic reactions were further confirmed by Raman spectroscopy (Figure 3b). Similarly, samples from different stage of preparation were analyzed. Sample I is the TiO_2@SiO_2 nanorod arrays. The Raman peaks at 399, 516, and 640 cm^{-1} are typically associated with anatase TiO_2.[18−20] Specifically, they are assigned to the Raman-active modes of anatase TiO_2 with B_1, A_{1g}, and E_g peaks, respectively. These Raman peaks are associated with symmetric bending vibration, antisymmetric bending vibration, and symmetric stretching vibration, respectively, of O−Ti−O in anatase TiO_2.[18−20] After magnesiothermic reduction, all the Raman peaks associated with anatase TiO_2 disappeared, suggesting TiO_2 has been converted to metallic Ti, in agreement with

DOI: 10.1021/acsami.5b00492
ACS Appl. Mater. Interfaces 2015, 7, 6867−6874

XRD analysis. The emergence of the Si Raman peaks after magnesiothermic reduction was clearly evidenced. The strongest peak at ~519 cm^{-1}, which is almost same as that from a typical Si wafer, could be associated with the Si−Si stretching mode in crystalline Si.[21,22] The broad small peak around 950 cm^{-1}, typically associated with Si−Si stretching mode in amorphous Si,[22] suggests the presence of amorphous Si as well. The Raman peaks associated with embedded MgO nanoparticles could be too weak or were suppressed by the dominant Raman peaks of Si.[23−26] The absence of MgO peaks is expected, as MgO has no measurable Raman modes between 200 and 900 cm^{-1} with the presence of other Raman-active materials and MgO can even be used as a Raman substrate with low background.[27] We also did control experiments to magnesiothermically reduce bare TiO_2 nanoarrays on titanium foil into metallic Ti nanorod arrays without the presence of SiO_2 coating (Figures S1 and S2 in Supporting Information). The metallic Ti nanorod arrays formed on metallic foils obtained from the control experiments could be used as 3-D current collector as well (Figure S6b in Supporting Information). The control experiments clearly show that (1) TiO_2 nanorod arrays could be magnesiothermically reduced to metallic Ti (evidenced by Raman with the disappearance of anatase TiO_2 peaks) and the morphology of the rodlike arrays was preserved, and (2) the Raman peak of Si in the Ti@Si nanorod arrays was from the Mg-reduced SiO_2 coating. In other words, the Raman analysis double-confirmed that the magnesiothermic reduction of both SiO_2 and TiO_2 was completed for the TiO_2@SiO_2 nanorod arrays. After HCl treatment, MgO was removed and the Si peaks were still observed as expected. After MgO attached was removed, the Raman peaks of Si associated with the second-order optical phonon modes 2TO (300 cm^{-1}) and second-order transverse acoustic phonon mode 2TA (945 cm^{-1}) further confirm the successful reduction of SiO_2 into Si.[28,29] The slight shift in position tower to smaller wavenumber of the first-order transverse optical phonon mode TO at 514 cm^{-1} after MgO removal could be attributed to the decreasing size of nanocrystallites and nanoporosity of the Si nanoshells after etching.[30] The absence of Raman signal of metallic Ti,[31−33] in contrast to that of XRD with notable Ti peaks, helps to easily identify the chemical compositions of samples obtained at different stages of synthesis. Therefore, on the basis of XRD and Raman analysis, we can confidently say that the outlined chemical changes as designed in Figure 1 were successfully achieved.

The structures of the intermediate products collected at each stage of synthesis were thoroughly characterized by FESEM (Figure 4). TiO_2 nanorod arrays could completely cover the Ti foil (Figure 4a,b). The length of nanorods is about 3 μm and the diameter is around 100 nm. The nanorods are not vertically attached on the Ti foil substrate, which could be attributed to the rough surface of the Ti foil used. Additionally, needlelike nanorods are observed. The mechanism of formation of TiO_2 nanorod arrays could be attributed to the topotactic transformation from the precursor $Na_2Ti_2O_5{\cdot}H_2O$.[8,34] Subsequent ion exchange could replace Na^+ with H^+, and a simple heat treatment could convert it to TiO_2 nanorods. The structure and arrangement allow each nanorod to be exposed to silica for effective coating. All the TiO_2 nanorod arrays were coated with silica, forming a uniform and smooth external surface (Figure 4c). The application of hydrolysis of TEOS to coat nanostructures with SiO_2 has been widely demonstrated for

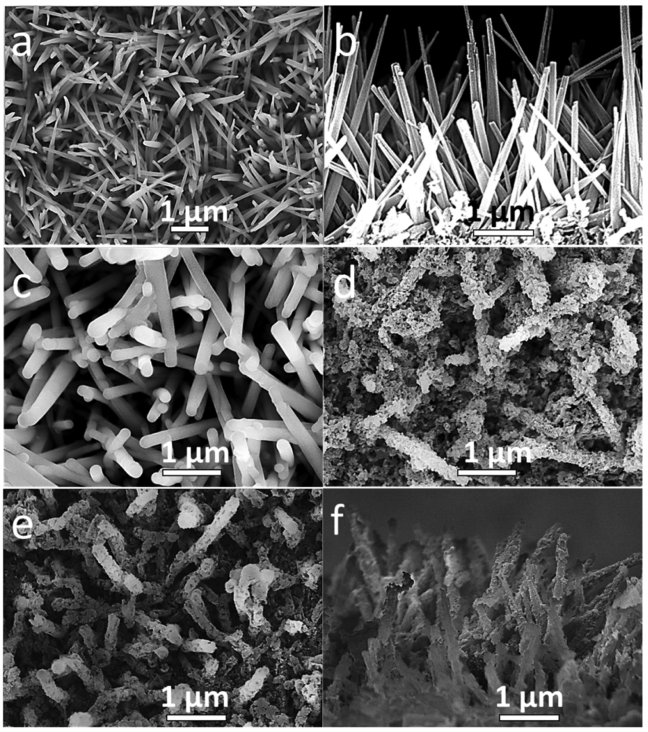

Figure 4. FESEM images of the series of nanorod arrays obtained at different stages of synthesis. (a) Top view of TiO_2 nanorod arrays grown on Ti foil after hydrothermal reaction. (b) Side view of sample a. (c) Top view of TiO_2@SiO_2 coaxial nanorod arrays after silica coating. (d) Ti/MgO@Si/MgO nanorod arrays after magnesiothermic reactions. (e) Top view of Ti@Si coaxial nanorod arrays on Ti foil after etching off MgO by HCl. (f) Side view of sample e.

various systems, such as Au@SiO_2 and Fe_3O_4@SiO_2 for diagnostic and therapeutic techniques, CdS@SiO_2 for photocatalytic applications, and CNT@SiO_2.[35,36]

Magnesiothermic reduction was carried out to simultaneously reduce both SiO_2 and TiO_2 into Si and Ti, respectively. The surface of the nanorods is highly rough after magnesiothermic reactions, which could be attributed to the attack of Mg and the formation of MgO on the nanorods. After etching by acid, MgO was almost removed. The surface of the nanorods is slightly smoother as compared to those with MgO nanoparticles. Additionally, one can note that there are defects/holes on the Ti@Si nanorods. The voids/defects could be attributed to the etching and removal of MgO on the nanorods generated from the replacement reactions between Mg with SiO_2 and TiO_2. Top- and side-view FESEM images (Figure 4e,f) suggest that the overall morphology of the Ti@Si nanorod arrays is still the same as the precursor TiO_2 nanorod arrays (Figure 4a,b). Low-magnification overall view shows that the nanorod arrays are distributed over the Ti substrates (Figure S5 in Supporting Information). Optical image showing the typical yellow to brown color of Si nanomaterials distributed on the substrate further confirms it (Figure S6 in Supporting Information).

TEM is employed to directly observe the morphology and to prove the existence of the core−shell structure (Figure 5). It can give a clear view of core−shell structures due to the differences in contrast for different compositions. Figure 5a clearly shows that the light-contrast silica layer was uniformly and firmly coated on the TiO_2 nanorod templates. There are some silica spheres as minor byproducts attached on the silica

DOI: 10.1021/acsami.5b00492
ACS Appl. Mater. Interfaces 2015, 7, 6867−6874

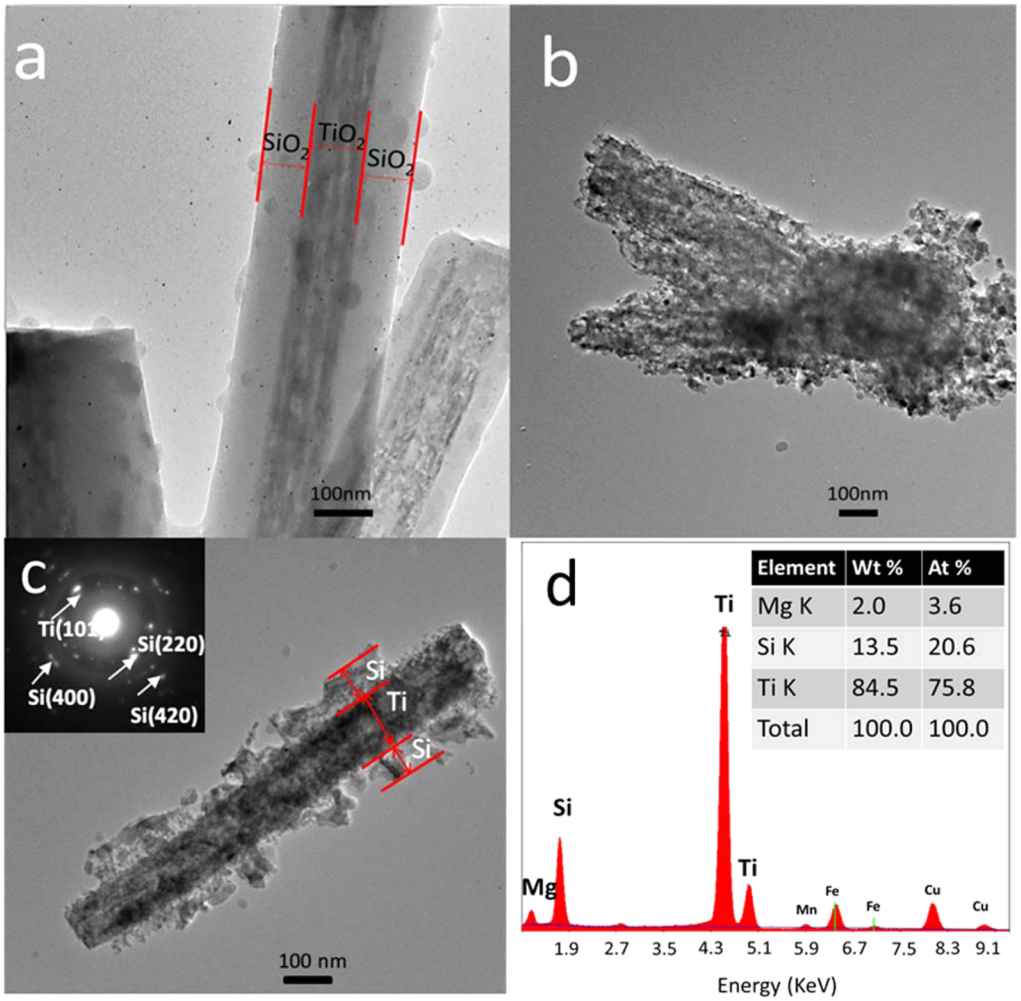

Figure 5. TEM images of the samples prepared after each step. (a) after silica coating of TiO_2 nanorods with SiO_2. (b) Ti/MgO@Si/MgO after Mg reduction. (c) Ti@Si after 0.5 M HCl treatment for 24 h (inset: SAED patterns of Si coating). (d) EDS results of panel c.

shells observed as well. After being reduced by Mg powders, a rough and porous structure of coating is observed (Figure 5b). Note that an excess amount of Mg powder was used and the roughness could be from the formation of MgO (Figure S3 in Supporting Information). The even contrast of the nanorods suggests that the MgO might be evenly distributed in the nanorods. Additional EDS analysis and elemental mapping also show the presence and distribution of Mg and other elements (Si, Ti, O) involved after magnesiothermic reactions (Figure S4 in Supporting Information). After treatment with 0.5 M HCl solution to remove MgO, the morphology of coating changed (Figure 5c), where the difference between Si and Ti is easily distinguishable. The selected-area electron diffraction (SAED) patterns (inset of Figure 5c) further confirm the formation of both Si and Ti. The diffraction from the lattice planes (220), (400), and (420) of Si and (101) of Ti could be indexed.

We also used electrochemical analysis to provide complementary characterization, in addition to XRD and Raman discussed previously, to identify the formed Si phase from reduced SiO_2 and the reduced TiO_2 phase into metallic Ti by magnesiothermic reduction. Cyclic voltammograms (CV) of Ti@Si nanorod arrays on Ti foil as the electrode were obtained and analyzed (Figure 6). The broad cathode peak at ~0.21 V could be attributed to the formation of amorphous Li_xSi phase.[37,38] Two anodic peaks, located at ~0.34 and ~0.49 V,

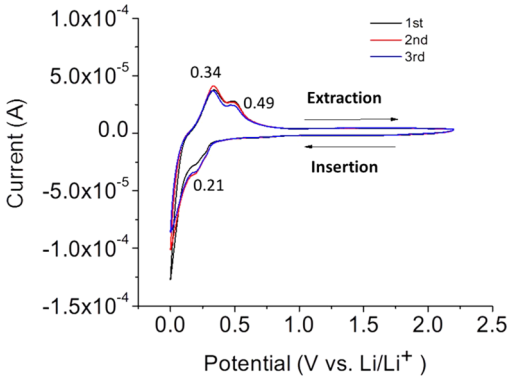

Figure 6. Cyclic voltammetry of Ti@Si nanorod arrays as electrode assembled into a standard half-cell and tested at ramp rate of 0.1 mV/s for three cycles.

correspond to the extraction of lithium ions from Li_xSi in the Ti@Si nanorod array electrode. The peaks and shape of the CV curve are consistent with the results reported previously in the literature for Si electrodes.[39−41] To be noted here, the characteristic peaks of TiO_2 at 1.65 and 2.15 V with the Ti^{4+}/Ti^{3+} redox couple during lithium insertion and extraction were not observed, which indirectly suggests that TiO_2 in the nanorods is reduced by Mg to lithium-inactive metallic Ti

DOI: 10.1021/acsami.5b00492
ACS Appl. Mater. Interfaces 2015, 7, 6867−6874

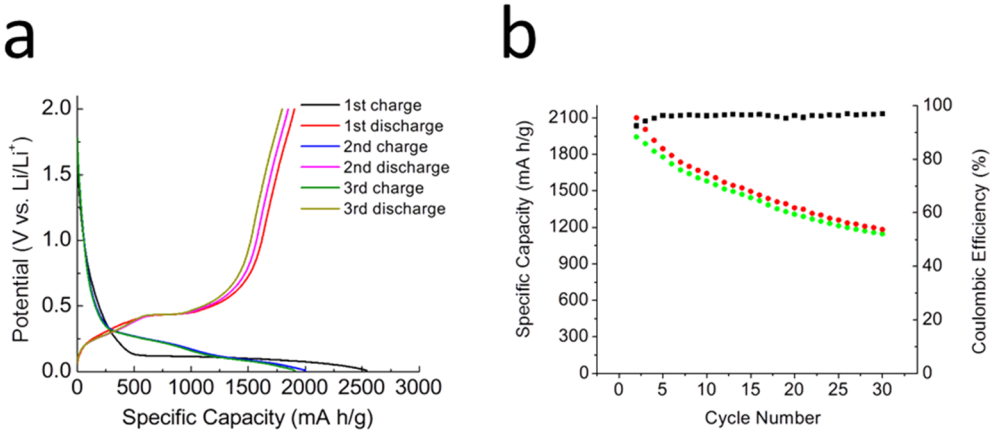

Figure 7. Electrochemical performance of Ti@Si nanorod arrays. (a) First three cycles of charge−discharge profiles tested at a current rate of 200 mA/g. (b) Capacity vs cycling number plot of Ti@Si nanorod arrays.

nanorods.[42] The CV could be considered as an electrochemical characterization tool, supplementary to those physical characterization tools.

Figure 7 shows the electrochemical performance of the Ti@Si nanorods cycled between 0.01 and 2 V at a galvanostatic current density of 200 mA/g. The profiles of the first three cycles are presented in Figure 7a. The first charge and discharge capacities of the electrode are 2540 and 1937 mA·h/g, respectively (Coulombic efficiency 76.3%). The first cycle Coulombic efficiency of 76.3% is much higher than those reported in the literature: the first cycle Coulombic efficiency is typically in the range 37−72%.[12,13,43−45] This irreversible capacity is attributed to the formation of the solid electrolyte interphase layer (SEI) during the first discharge process.[3,38] As the cycling progressed, the ions transportation would be partly affected by the SEI layer. As the result, the reversible capacity decreased gradually, possibly due to the electrode disintegration.[1] A capacity of 1125 mA·h/g was retained after 30 cycles. Coulombic efficiency of ∼95% during the cycling could be maintained, indicating reasonably good stability for silicon in our Ti@Si electrodes. The improved electrochemical performance is mainly ascribed to its special 3D architecture. The porous Si coating clings strongly to the metallic Ti nanorods, leading to improved electrode conductivity and structural stability. Additionally, the unique 1D core−shell structure has space to accommodate the large volume change in charge−discharge process. As one can notice, the capacity fading is still significant for our not-optimized samples. There are a few approaches to explore in order to further address the capacity fading of Si, such as (1) to coat the external Si surface with a protective layers, for example, carbon; (2) to stabilize the SEI on Si surface by introducing electrolyte additives, for example, fluoroethylene carbonate; or (3) to decorate the Si surface with highly conductive materials, for example, Ag nanoparticles. Our ongoing effort is to optimize the conditions and further improve the performance using the same Ti@Si nanorod design.

CONCLUSIONS

We have introduced a facile procedure to fabricate the unique core−shell Ti@Si nanorod arrays on Ti foils as integrated electrodes without any postsynthesis treatment for LIBs and achieved improved performances. The strategy could be further expanded to prepare other 3-D structured Si-based electrodes (e.g., CNT@Si nanoarrays) for batteries. We demonstrated the feasibility of using the magnesiothermically synthesized Si@Ti nanorods as a promising silicon anode material. The Ti@Si nanorod arrays on Ti foils with metallic and conductive Ti cores could deliver a decent capacity of 1125 mA·h/g for at least 30 cycles. We also demonstrated that it would be possible to prepare metallic Ti nanorod arrays by magnesiothermic reaction, which may find other applications (e.g., 3-D current collectors).The strategy outlined in this paper could be employed for the preparation of other coaxial core−shell 1-D nanomaterials. Our ongoing efforts are to optimize the magnesiothermic reduction process and to explore the general application of this approach.

ASSOCIATED CONTENT

Supporting Information

Six figures showing FESEM images and Raman spectra of bare Ti nanorod arrays derived from magnesiothermically reduced TiO_2 nanoarrays on titanium foils and additional characterization and minor structures observed of the intermediate component of Ti/MgO@Si/MgO and coaxial Ti@Si nanorod arrays. This material is available free of charge via the Internet at http://pubs.acs.org.

AUTHOR INFORMATION

Corresponding Author

*E-mail da.deng@wayne.edu.

Author Contributions

D.D. designed the experiments; X.H. carried out the experiments; D.D. and X.H. analyzed the results and wrote the paper.

Notes

The authors declare no competing financial interest.

ACKNOWLEDGMENTS

We appreciate the discussion with Dr. Xingcheng Xiao from General Motors Global R&D Center. The Lumigen Instrument Center, Wayne State University, is appreciated.

REFERENCES

(1) Szczech, J. R.; Jin, S. Nanostructured Silicon for High Capacity Lithium Battery Anodes. *Energy Environ. Sci.* **2011**, *4*, 56−72.

(2) Boukamp, B. A.; Lesh, G. C.; Huggins, R. A. All-Solid Lithium Electrodes with Mixed-Conductor Matrix. *J. Electrochem. Soc.* **1981**, *128*, 725.

DOI: 10.1021/acsami.5b00492
ACS Appl. Mater. Interfaces 2015, 7, 6867−6874

(3) Wu, H.; Chan, G.; Choi, J. W.; Ryu, I.; Yao, Y.; McDowell, M. T.; Lee, S. W.; Jackson, A.; Yang, Y.; Hu, L. B.; Cui, Y. Stable Cycling of Double-Walled Silicon Nanotube Battery Anodes through Solid-Electrolyte Interphase Control. *Nat. Nanotechnol.* **2012**, *7*, 309−314.
(4) Hu, Y. S.; Rezan, D. C.; Titirici, M. M.; Muller, J. O.; Schlogl, R.; Antonietti, M.; Maier, J. Superior Storage Performance of a Si@SiOx/C Nanocomposite as Anode Material for Lithium-Ion Batteries. *Angew. Chem., Int. Ed.* **2008**, *47*, 1645−1649.
(5) Fan, Y.; Huang, K.; Zhang, Q.; Xiao, Q. Z.; Wang, X. H.; Chen, X. D. Novel Silicon-Nickel Cone Arrays for High Performance LIB Anodes. *J. Mater. Chem.* **2012**, *22*, 20870−20873.
(6) Wang, D. S.; Yang, Z. B.; Li, F.; Wang, X. H.; Liu, D. Q.; Wang, P.; He, D. Y. Performance of Si-Ni Nanorod as Anode for Li-Ion Batteries. *Mater. Lett.* **2011**, *65*, 3227−3229.
(7) Liu, B.; Deng, D.; Lee, J. Y.; Aydil, E. S. Oriented Single-Crystalline TiO_2 Nanowires on Titanium Foil for Lithium Ion Batteries. *J. Mater. Res.* **2010**, *25*, 1588−1594.
(8) Liu, B.; Boercker, J. E.; Aydil, E. S. Oriented Single Crystalline Titanium Dioxide Nanowire. *Nanotechnology* **2008**, *19*, No. 505604.
(9) Bao, Z. H.; Weatherspoon, M. R.; Shian, S.; Cai, Y.; Graham, P. D.; Allan, S. M.; Ahmad, G.; Dickerson, M. B.; Church, B. C.; Kang, Z. T.; Abernathy, H. W.; Summers, C. J.; Liu, M. L.; Sandhage, K. H. Chemical Reduction of Three-Dimensional Silica Micro-Assemblies into Microporous Silicon Replicas. *Nature* **2007**, *446*, 172−175.
(10) Richman, E. K.; Kang, C. B.; Brezesinski, T.; Tolbert, S. H. Ordered Mesoporous Silicon through Magnesium Reduction of Polymer Templated Silica Thin Films. *Nano Lett.* **2008**, *8*, 3075−3079.
(11) Chen, K.; Bao, Z. H.; Du, A.; Zhu, X. R.; Wu, G. M.; Shen, J.; Zhou, B. Synthesis of Resorcinol-Formaldehyde/Silica Composite Aerogels and Their Low-Temperature Conversion to Mesoporous Silicon Carbide. *Microporous Mesoporous Mater.* **2012**, *149*, 16−24.
(12) Choi, S.; Lee, J. C.; Park, O.; Chun, M. J.; Choi, N. S.; Park, S. Synthesis of Micro-Assembled Si/Titanium Silicide Nanotube Anodes for High-Performance Lithium-Ion Batteries. *J. Mater. Chem. A* **2013**, *1*, 10617−10621.
(13) Zhu, S. M.; Zhu, C. L.; Ma, J.; Meng, Q.; Guo, Z. P.; Yu, Z. Y.; Lu, T.; Li, Y.; Zhang, D.; Lau, W. M. Controlled Fabrication of Si Nanoparticles on Graphene Sheets for Li-Ion Batteries. *RSC Adv.* **2013**, *3*, 6141−6146.
(14) Guo, S.; Li, H. X.; Bai, H. M.; Tao, Z. L.; Chen, J. Ti/Si/Ti Sandwich-Like Thin Film as the Anode of Lithium-Ion Batteries. *J. Power Sources* **2014**, *248*, 1141−1148.
(15) Zhang, R. Y.; Du, Y. J.; Li, D.; Shen, D. K.; Yang, J. P.; Guo, Z. P.; Liu, H. K.; Elzatahry, A. A.; Zhao, D. Y. Highly Reversible and Large Lithium Storage in Mesoporous Si/C Nanocomposite Anodes with Silicon Nanoparticles Embedded in a Carbon Framework. *Adv. Mater.* **2014**, *26*, 6749−6755.
(16) Bolívar, M. S. R.; Friedrich, I. B. Synthesis of Titanium via Magnesiothermic Reduction of TiO_2 (Pigment). Proceedings of Electronic Materials Conference, University Park, PA, June 24−26, 2009.
(17) Li, W. N.; Ding, Y. S.; Yuan, J. K.; Gomez, S.; Suib, S. L.; Galasso, F. S.; DiCarlo, J. F. Synthesis and Characterization of Silicon Nanowires on Mesophase Carbon Microbead Substrates by Chemical Vapor Deposition. *J. Phys. Chem. B* **2005**, *109*, 3291−3297.
(18) Ohsaka, T.; Izumi, F.; Fujiki, Y. Raman Spectrum of Anatase, TiO_2. *J. Raman Spectrosc.* **1978**, *7*, 321−324.
(19) Tian, F.; Zhang, Y. P.; Zhang, J.; Pan, C. X. Raman Spectroscopy: A New Approach to Measure the Percentage of Anatase TiO_2 Exposed (001) Facets. *J. Phys. Chem. C* **2012**, *116*, 7515−7519.
(20) Zhang, J.; Li, M. J.; Feng, Z. C.; Chen, J.; Li, C. UV Raman Spectroscopic Study on TiO_2. I. Phase Transformation at the Surface and in the Bulk. *J. Phys. Chem. B* **2006**, *110*, 927−935.
(21) Lewis, I. R.; Edwards, H. G. M. *Handbook of Raman Spectroscopy: From the Research Laboratory to the Process Line*; Marcel Dekker: New York, 2001.
(22) Liu, X. L.; Gao, Y. F.; Jin, R. H.; Luo, H. J.; Peng, P.; Liu, Y. Scalable Synthesis of Si Nanostructures by Low-Temperature Magnesiothermic Reduction of Silica for Application in Lithium Ion Batteries. *Nano Energy* **2014**, *4*, 31−38.
(23) Kim, H. S.; Kim, H. W. Fabrication and Raman Studies of MgO/SnO_2 Core-Shell Heteronanowires. *Acta Phys. Polym., A* **2009**, *116*, 58−61.
(24) Ishikawa, K.; Fujima, N.; Komura, H. First Order Raman Scattering in MgO. *J. Appl. Phys.* **1985**, *57*, 973−975.
(25) Bockelmann, H. K.; Schlecht, R. G. Raman Scattering from Microcrystals of MgO. *Phys. Rev.* **1974**, *10*, 5225−5231.
(26) Li, Q. W.; Yan, H.; Cheng, Y.; Zhang, J.; Liu, Z. F. A Scalable CVD Synthesis of High-Purity Single-Walled Carbon Nanotubes with Porous MgO as Support Material. *J. Mater. Chem.* **2002**, *12*, 1179−1183.
(27) Gasparov, L.; Jegorel, T.; Loetgering, L.; Middey, S.; Chakhalian, J. Thin Film Substrates from the Raman Spectroscopy Point of View. *J. Raman Spectrosc.* **2014**, *45*, 465−469.
(28) Yu, D. P.; Bai, Z. G.; Ding, Y.; Hang, Q. L.; Zhang, H. Z.; Wang, J. J.; Zou, Y. H.; Qian, W.; Xiong, G. C.; Zhou, H. T.; Feng, S. Q. Nanoscale Silicon Wires Synthesized Using Simple Physical Evaporation. *Appl. Phys. Lett.* **1998**, *72*, 3458−3460.
(29) Wang, R. P.; Zhou, G. W.; Liu, Y. L.; Pan, S. H.; Zhang, H. Z.; Yu, D. P.; Zhang, Z. Raman Spectral Study of Silicon Nanowires: High-Order Scattering and Phonon Confinement Effects. *Phys. Rev.* **2000**, *61*, 16827−16832.
(30) Kanemitsu, Y.; Uto, H.; Masumoto, Y.; Matsumoto, T.; Futagi, T.; Mimura, H. Microstructure and Optical-Properties of Freestanding Porous Silicon Films - Size Dependence of Absorption-Spectra in Si Nanometer-Sized Crystallites. *Phys. Rev.* **1993**, *48*, 2827−2830.
(31) Xu, C. L.; Geng, H. W.; Bennett, R.; Clayton, D. A.; Pan, S. L. Ti@TiO_2 Nanowire Electrode with Polydisperse Gold Nanoparticles for Electrogenerated Chemiluminescence and Surface Enhanced Raman Spectroelectrochemistry. *J. Phys. Chem. C* **2013**, *117*, 1849−1856.
(32) Mantzila, A. G.; Prodromidis, M. I. Development and Study of Anodic Ti/TiO_2 Electrodes and Their Potential Use as Impedimetric Immunosensors. *Electrochim. Acta* **2006**, *51*, 3537−3542.
(33) Peng, X. S.; Wang, J. P.; Thomas, D. F.; Chen, A. C. Tunable Gowth of TiO_2 Nanostructures on Ti Substrates. *Nanotechnology* **2005**, *16*, 2389−2395.
(34) Chen, W. P.; Guo, X. Y.; Zhang, S. L.; Jin, Z. S. TEM Study on the Formation Mechanism of Sodium Titanate Nanotubes. *J. Nanopart. Res.* **2007**, *9*, 1173−1180.
(35) Andrés, G. M.; Jorge, P. J.; Luis, M. L. M. Recent Progress on Silica Coating of Nanoparticles and Related Nanomaterials. *Adv. Mater.* **2010**, *22*, 1182−1195.
(36) Seeger, T.; Redlich, P.; Grobert, N.; Terrones, M.; Walton, D. R. M.; Kroto, H. W.; Ruhle, M. SiOx-Coating of Carbon Nanotubes at Room Temperature. *Chem. Phys. Lett.* **2001**, *339*, 41−46.
(37) Obrovac, M. N.; Krause, L. J. Reversible Cycling of Crystalline Silicon Powder. *J. Electrochem. Soc.* **2007**, *154*, A103−A108.
(38) Chan, C. K.; Peng, H. L.; Liu, G.; McIlwrath, K.; Zhang, X. F.; Huggins, R. A.; Cui, Y. High-Performance Lithium Battery Anodes Using Silicon Nanowires. *Nat. Nanotechnol.* **2008**, *3*, 31−35.
(39) Ge, M. Y.; Rong, J. P.; Fang, X.; Zhou, C. W. Porous Doped Silicon Nanowires for Lithium Ion Battery Anode with Long Cycle Life. *Nano Lett.* **2012**, *12*, 2318−2323.
(40) Kim, H.; Cho, J. Superior Lithium Electroactive Mesoporous Si@Carbon Core-Shell Nanowires for Lithium Battery Anode Material. *Nano Lett.* **2008**, *8*, 3688−3691.
(41) Zhang, H. G.; Braun, P. V. Three-Dimensional Metal Scaffold Supported Bicontinuous Silicon Battery Anodes. *Nano Lett.* **2012**, *12*, 2778−2783.
(42) Wang, Y. F.; Wu, M. Y.; Zhang, W. F. Preparation and Electrochemical Characterization of TiO_2 Nanowires as an Electrode Material for Lithium-Ion Batteries. *Electrochim. Acta* **2008**, *53*, 7863−7868.
(43) Tang, Y. Y.; Xia, X. H.; Yu, Y. X.; Shi, S. J.; Chen, J.; Zhang, Y. Q.; Tu, J. P. Cobalt Nanomountain Array Supported Silicon Film

DOI: 10.1021/acsami.5b00492
ACS Appl. Mater. Interfaces 2015, 7, 6867−6874

Anode for High-Performance Lithium Ion Batteries. *Electrochim. Acta* **2013**, *88*, 664−670.
(44) Ng, S. H.; Wang, J. Z.; Wexler, D.; Konstantinov, K.; Guo, Z. P.; Liu, H. K. Highly Reversible Lithium Storage in Spheroidal Carbon-Coated Silicon Nanocomposites as Anodes for Lithium-Ion Batteries. *Angew. Chem., Int. Ed.* **2006**, *45*, 6896−6899.
(45) Luo, J. Y.; Zhao, X.; Wu, J. S.; Jang, H. D.; Kung, H. H.; Huang, J. X. Crumpled Graphene-Encapsulated Si Nanoparticles for Lithium Ion Battery Anodes. *J. Phys. Chem. Lett.* **2012**, *3*, 1824−1829.

DOI: 10.1021/acsami.5b00492
ACS Appl. Mater. Interfaces 2015, 7, 6867−6874